International Journal on Interactive Design and Manufacturing (IJIDeM)
https://doi.org/10.1007/s12008-023-01419-0

ORIGINAL PAPER

Computational analysis of a new airfoil for micro-capacity wind turbine

Minendra L. Surve[1] · Prashant D. Deshmukh[1] · Kailasnath B. Sutar[2] · Bharatbhushan S. Kale[3] · Kiran Suresh Bhole[4]

Received: 18 April 2023 / Accepted: 26 June 2023

Abstract
The wind and the solar energy are the most reliable origins of sustainable energy. A small wind turbine is one of the most reliable and effective sources of generation of electricity at remote locations. Micro-capacity wind turbines operating at low wind speeds result in poor performance because of the detachment of air on the cutting edge of the blades. Use of specially designed airfoils for operation at low Reynolds number ($Re = 5 \times 10^5$) permits energizing at low airstream. It helps to increase the start-up torque and the overall performance of the wind turbine. A new airfoil INDTH8 is designed using QBlade software and its performance is compared computationally with four different airfoils viz. E180, NACA 2408, ONERA OA209, and SD5060. The airfoil INDTH8 is analyzed computationally for a 3-bladed rotor having a diameter of 2.4 m. Blade Element Momentum theory is used for the design of the 3-bladed rotor. From QBlade simulation, it is found that at an average wind speed of 7 m/s, the maximum power coefficient (C_P) is 0.522. It is also found that at different rotational speeds viz. 200 rpm, 300 rpm, 400 rpm, and 500 rpm, the maximum obtainable powers are about 177 W, 441 W, 498 W, and 447 W respectively at a tip speed ratio of 7.

Keywords Micro-capacity · Wind turbine · QBlade · Airfoil · BEM theory · Lift to drag ratio

1 Introduction

By the end of the year 2021, the share of renewable energy increased to 38% of the global installed capacity. In the year 2021, globally 93 GW of wind energy capacity was added, taking the total global wind power installed capacity to 824.87 GW [1]. India has total wind power installed capacity of 42.6 GW till 31st March, 2023 [2]. Wind turbine is the appliance that converts the kinetic energy of the wind into mechanical energy and further into electrical power. Wind turbines are mostly classified into two categories viz. horizontal axis wind turbines (HAWT) and vertical axis wind turbines (VAWT). The blades of HAWT consist of airfoil cross-section. It results in lift and drag forces due to the pressure differences across the two-dimensional airfoil. The production of electricity from wind is not only reasonably priced but also resource-efficient [3]. Table 1 reports categories of wind turbines based on their capacities for power generation.

The region that receives an annual average wind speed of up to 6 m/s is suitable for producing power up to 15 kW, having swept area of 80 m^2. Tummala et al. [4] conducted a review of the literature on small-size wind turbines and concluded that the airfoil is the truly important part of wind turbine rotor blades.

The airfoil is the cross-sectional shape of the blade (Fig. 1). Aerodynamic shape as well as the structural performance of the airfoil evaluates the energy-capturing practice of the

✉ Kailasnath B. Sutar
kbsutar@bvucoep.edu.in

Minendra L. Surve
minendrasurve@gmail.com

Prashant D. Deshmukh
pddeshmukh7@gmail.com

Bharatbhushan S. Kale
bhrtkale18@gmail.com

Kiran Suresh Bhole
kiranbhole1977@gmail.com

1 Datta Meghe College of Engineering, Navi Mumbai 400708, India

2 Bharati Vidyapeeth (Deemed To Be University) College of Engineering, Pune 411043, India

3 Fr. C. Rodrigues Institute of Technology, Vashi, Navi Mumbai 400703, India

4 Sardar Patel College of Engineering, Andheri, Mumbai 400058, India

Published online: 11 July 2023

Table 1 Categorization of wind turbines based on capacity of power generation [4, 5]

Scale	Capacity
Micro	4–250 W
Mini	251–16 kW
Small	17–100 kW
Medium	101–999 kW
Large	1–3 MW
Ultra large	Above 3 MW

blade. Suction is induced on the upper side of the airfoil, where velocity is higher than static pressure; due to this effect, the lift is generated.

QBlade software is used to design and simulate wind turbines. It is available under an academic public license for non-commercial use [6]. Marten et al. [7] developed QBlade software. According to the authors, QBlade utilizes the Blade Element Momentum (BEM) method for simulation of horizontal axis wind turbines. During simulation in QBlade software, the set of equations found from the relationship between the blade forces and flow momentum are solved iteratively. In QBlade software, XFOIL an interactive program for the design and analysis of subsonic isolated airfoils is used [8]. Many researchers have used QBlade software for simulation of wind turbine blades [9, 10].

Giguere and Seilg [11] found that the airfoils designed thinner than conventional airfoils were suitable for the use of high Reynolds numbers also. The low Reynolds number and the centrifugal stiffening effects provide optimal performance for small wind turbines. Hence, small wind turbines run at low Reynolds numbers. Lee et al. [12] designed two types of blades: one based on the BEM theory and another with a constant chord length. The results of experimentation and numerical simulations give out that the maximal power coefficient for the blade designed using BEM theory rises up by 50% compared with the baseline blade. The blade designed based on BEM theory had a fully attached flow over the airfoil without separation. The authors found that the rotor blade designed based on BEM theory had a power coefficient higher than that of the baseline blade at low tip speed ratios. Akour et al. [13] and Almohammadi et al. [14] reported that lift coefficient (C_L), drag coefficient (C_D), lift-to-drag ratio (C_L/C_D), and stall play very important roles in improved aerodynamic performance in case of a small capacity wind turbines.

The design of airfoils and blades plays an important role to get sufficient output from the wind turbine [15]. Singh et al. [16] predicted that the power coefficient (C_p) has an effective relationship with C_L/C_D ratio; the larger the C_L/C_D ratio, the higher the C_p. Karasu et al. [17] performed experimentation and numerical investigation on NACA2415 and NACA4412 airfoils and found that changing both the thickness and camber ratio of airfoils reduce the laminar separation and finally the aerodynamic losses. Power coefficient is measurable parameter for wind turbine; it increases with an increase in the thickness of the airfoil [18, 19].

In the present work, the authors have used QBlade software for the design and analysis of a new airfoil viz. INDTH8 for a micro-capacity wind turbine. The performance of the new airfoil INDTH8 and the rotor blades is compared computationally with four different airfoils *viz.* E180, NACA 2408, ONERA OA209, and SD5060 that are selected from the airfoil database [20–23]. A wind turbine converts kinetic energy of wind into a mechanical energy which is further converted into electrical energy. The extractable or useful power (P_u) from the wind is reported by Manwell et al. [5] as follows.

At steady state flow and energy conservation takes place.

The energy required for displacing the object from its rest position to distance s by the application of force$F$ is given as:

$$E = F.s \tag{1}$$

According to Newton's 2nd law of motion, based on the assumption that the object has a constant mass:

$$F = ma \tag{2}$$

$$E = mas \tag{3}$$

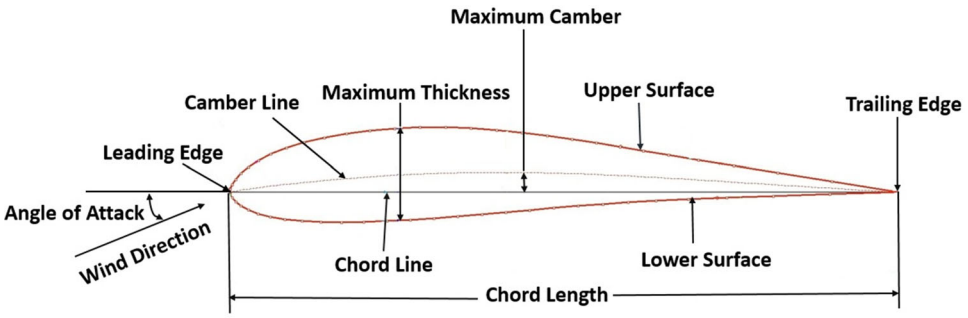

Fig. 1 Geometry of a typical airfoil

Using the 3rd equation of motion, which is derived from the 1st and 2nd equations of motion,

$$V^2 = u^2 + 2as \tag{4}$$

$$\text{Weget} : a = \left(V^2 - u^2\right)/2s \tag{5}$$

Here initial velocity of object is zero, i.e.

$$u = 0,\ a = V^2/2s \tag{6}$$

Substitute it in Eq. (3) we get:

$$E = {}^1/_2 m\, V^2 \tag{7}$$

Now, rate of energy per unit time i.e. power

$$P = dE/dt = {}^1/_2 V^2 dm/dt \tag{8}$$

$$dm/dt = \rho\, A dx/dt \tag{9}$$

$$\text{As}\, dx/dt = V,\ dm/dt = \rho A\, V \tag{10}$$

Then, Eq. (8) becomes,

$$P = {}^1/_2 \rho\, A\, V^3 \tag{11}$$

But, according to Betz's limit, only a fraction of total wind power can be extracted as a useful power. Hence,

$$P_u = {}^1/_2 \rho A V^3 Cp \tag{12}$$

where, ρ: air density (kg/m^3); A: rotor swept area (m^2); V: wind velocity (m/s); C_p: power coefficient.

2 Design of a new airfoil

To obtain higher efficiency of micro-capacity wind turbines in low air stream location, the starting torque of the turbine has to be high. This is possible at best when streamlined accomplishment of the blades is higher i.e. the aerodynamic losses are minimum.

The computational studies on the new airfoil involve the variations in C_L, C_D, C_L/C_D, C_M, and C_p at different angles of attack (AOA) using QBlade software. The range AOA is taken from 0° to 20°.

In all, 62 dimensional coordinates are taken for the design of the advanced airfoil. Mach number is taken as zero for the present study. The value of the *Ncrit* number is chosen as 9 which represent the normal wind tunnel circumstances [24]. The range of Reynolds number is taken from 1×10^5 to 5×10^5 and the Mach number is considered to be zero.

Table 2 reports a comparison of the different design parameters for the five airfoils under consideration.

It is clear from Table 2 that the newly designed airfoil INDTH8 shows a maximum C_L/C_D of 89.86 which is higher than the remaining four airfoils. It is also figured out that the optimum angle of attack at maximum C_L/C_D is 7° whereas, for maximum *CL*, it is 13.5°. The variation in torque coefficient (*CM*) with AOA for the new airfoil shows that with the increase in AOA, the torque coefficient increases gradually up to an AOA of 10°. From AOA of 10° to 14°, there is a sharp increase in torque coefficient. For further increase in AOA, there is a sudden decrease in torque coefficient. The new airfoil (INDTH8) has a maximum thickness of 8.87% and maximum camber of 6.07%. The IND means India, TH means the thickness of the airfoil, and the last digit indicates the thickness i.e. 8 mm. Fig. 2 reports a comparison among all five types of airfoils in graphical form. Camber length is maximum for the airfoil INDTH8 whereas minimum for the airfoil ONERA OA209. According to Yining [25], the drag, lift, and the lift-to-drag ratio rises with the camber length whereas the angle of attack (AOA) corresponding to the maximum lift-to-drag ratio decreases. The QBlade simulation results obtained for all the airfoils in present study are in line with those obtained by Yining [25].

A comparison of the lift coefficient (C_L) versus the angle of attack (α) for INDTH8 airfoil with the four airfoils under the study at $Re = 500{,}000$. The INDTH8 airfoil shows better results among all the airfoils. For the INDTH8 airfoil, the lift coefficient increases from 0.6 at an AOA of 0° to

1.68 at an AOA of 13.5°. The stall angles for airfoils E180, NACA2408, ONERAOA209, SD5060 is found to be 10.5°, 10°, 14° and 11° respectively. According to Osei et al. [26], cutback in lift coefficient beyond maximum lift coefficient is due to occurrence of stall condition.

The plot of lift to drag ratio (C_L/C_D) versus angle of attack (α) (Fig. 3) shows that for AOA of 0° to 7°, there is an increase in a lift to drag ratio from 55.84 to 89.87. As the AOA increases beyond 7° there is a decrease in C_L/C_D ratio. The point beyond which C_L/C_D ratio falls gradually is called as the stall point. At the stall point, the flow separation takes place which results in a gradual decrease in C_L/C_D ratio. Here, the speed of the fluid flow in the boundary layer region approaches zero relative to that of the wind turbine rotor blade. Flow detachment fallout from the surface of the blade due to the formation of vortices and eddies occurs that cause increase in drag. The result obtained for the INDTH8 airfoil is in line with those obtained by Kale et al. [27].

From the comparative analysis of all the airfoils, it is found that the newly designed INDTH8 airfoil shows that at an angle of attack of 7°, the maximum value of C_L/C_D ratio obtained is 89.87. The C_L/C_D ratio versus AOA signifies the

Table 2 Comparison among the airfoils for different design parameters

Type of AIRFOIL	Max. thickness (% chord length)	Max. chamber (% chord length)	AOA at max *CL*/*CD*	Max. *CL*/*CD*	AOA at max. *CL*	Max. *CL*
INDTH8	8.87	6.07	7	89.87	13.5	1.68
E180	8.58	2.24	4	86.78	10.5	1.14
NACA 2408	8	2	4	87.78	10	1.15
ONERA OA209	9.01	1.56	8	75.77	14	1.38
SD5060	9.46	2.30	4	89.54	11	1.32

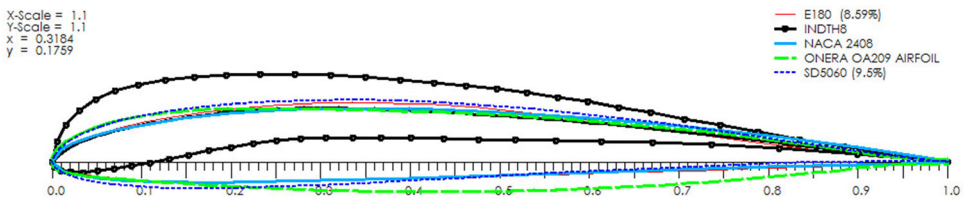

Fig. 2 Different shapes of airfoils in QBlade software

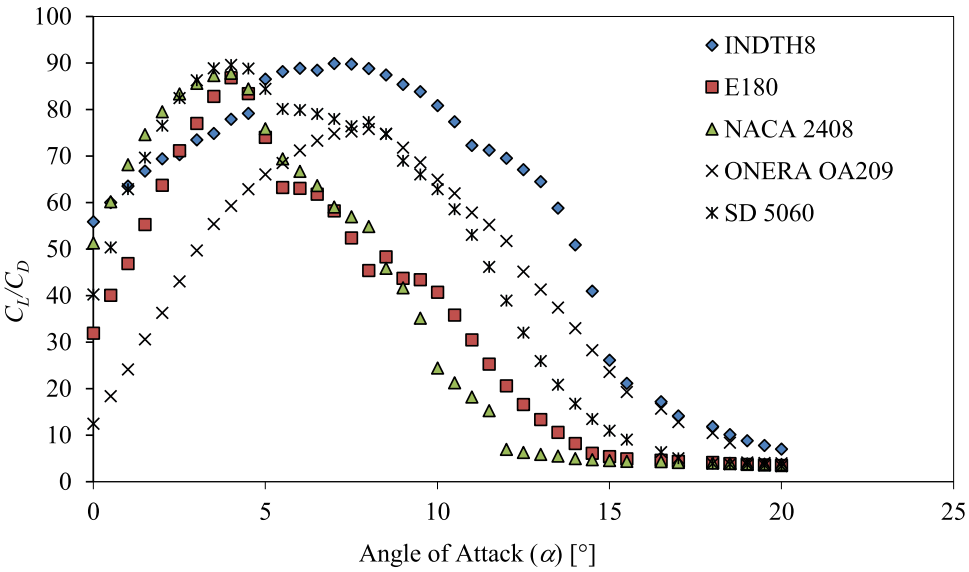

Fig. 3 Plot of lift to drag ratio versus angle of attack

maximum lift force for that of the drag force generated by the airfoil. Similarly, for the airfoils E180, NACA 2408, ONERA OA209, and SD5060 the maximum C_L/C_D ratios of 86.78, 87.78, 75.77, and 89.54 are obtained at AOAs of 4°, 4°, 8°, and 4° respectively.

Figure 4 reports a comparison of the (C_L/C_D) ratio versus the Reynolds Number (*Re*) for the different airfoils. It is found for all five airfoils that the (C_L/C_D) ratio increases as the *Re* increases from 100,000 to 500,000. This is owing to the increased gust speed corresponding to the *Re*. According to Osei et al. [26], there were no notable changes in lift coefficient at $Re \geq 300{,}000$. Lee and Lee [28] reported that this practice is in consequence to non-linear aerodynamic characteristics that is analogous with the low Re set-up. The simulation results obtained for all five airfoils under present study are in line with those obtained by Osei et al. [26]. Newly designed airfoil INDTH13 for micro-capacity application at low Reynolds region Re ranging from (200,000–500,000) makes it worthy to use. The results obtained in this study for INDTH8 airfoil are in line with those obtained by Surve et al. [29].

3 Turbine simulation

Figure 5 shows the flow chart employ in the entire work of wind turbine blade design and simulation. The design of HAWT is conducted using the QBlade tool. To design

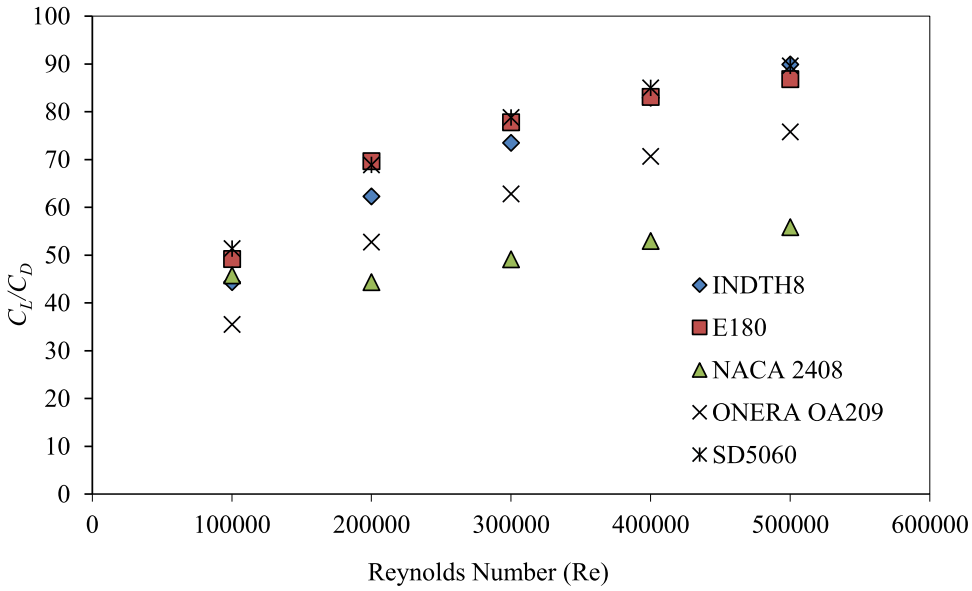

Fig. 4 Plot of lift to drag ratio versus Reynolds number

a new airfoil, the airfoil parameters such as height, chord and radius are inserted in the software for Xfoil analysis. The design parameters such as lift coefficient C_L, drag coefficient C_D, and momentum coefficient C_M at different AOAs are obtained. The next stage is to design a rotor blade by utilizing the Blade Element Moment (BEM) theory. The blade characteristics like chord length, twist angle, and the number of blades are inserted in the software. Once all input parameters are given to the software, the boundary conditions are applied and a flow field simulation is generated. After performing the rotor simulation, the output parameters such as power coefficient C_P and thrust coefficient C_T are computed for different Tip Speed Ratios (TSR). If the power coefficient (C_P) approaches Betz's limit i.e. 0.593 then the wind turbine blade is satisfying the aspects of blade design. Now, the user can proceed with the dimensions corresponding to the blade design for manufacturing. If the C_P does not approach Betz's limit let's say 0.5 then the wind turbine blade is needed to be redesigned till valid outcomes are found. Table 3 reports the characteristics of the rotor blade simulated from the new airfoil INDTH8.

Manwell et al. [5] reported local tip speed ratio as:

$$\lambda_r = \lambda \frac{r}{R} \tag{13}$$

where, λ: Tip Speed Ratio, r: Local radius and R: Rotor radius or blade span.

For first element with local radius $r = 200$ mm, rotor radius $R = 1200$ mm, and TSR 7, local tip speed ratio is given as:

$$\lambda_{200} = 7 \times \frac{200}{1200} = 1.17$$

To calculate the relative angle φ corresponding to the each element of blade and can be given as:

$$\varphi = \frac{2}{3}\tan^{-1}\left(\frac{1}{\lambda_r}\right) \tag{14}$$

$$\varphi = \frac{2}{3}\tan^{-1}\left(\frac{1}{1.17}\right) = 27.01^\circ$$

Chord length (C) can be calculated as:

$$C = \frac{8\pi r}{BC_{l,}}(1 - \cos\varphi) \tag{15}$$

Here, B: number of blades (3 for the present case), $C_L = 1.29$ and r: 200 mm. Then,

$$C = \frac{8 \times \pi \times 200}{3 \times 1.29}(1 - \cos 27.01) = 141.67\,\text{mm}$$

Solidity (σ') is describe as the ratio of blade area to swept area. Mathematically,

$$\sigma' = \frac{BC}{2\pi r} = \frac{3 \times 141.67}{2 \times \pi \times 200} = 0.34 \tag{16}$$

The effect of tangential flow imparted by blades on the wind is known as wake rotation. To understand this phenomenon considering the coefficient of drag ($C_D = 0$) and tip deprivation ($F = 1$). Here, F is Prandtl's tip loss factor; this signifies that there is no tip loss [30, 31].

The axial induction factor (a) which is the partial decrease in axial component of wind velocity between the freestream

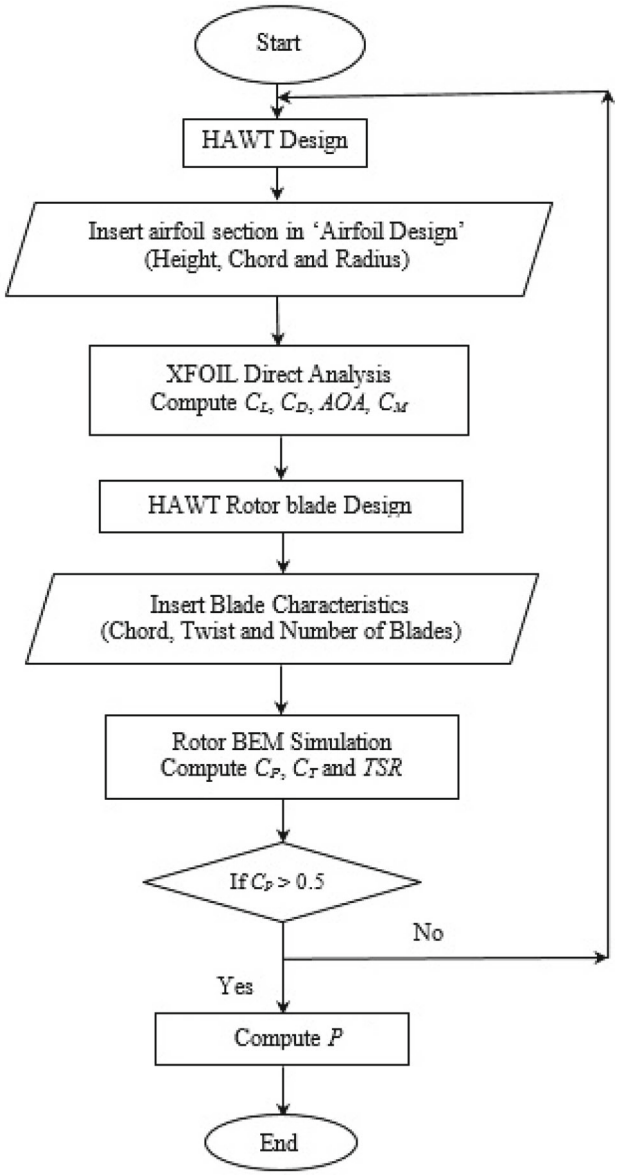

Fig. 5 Flow chart for wind turbine blade design and simulation

Table 3 Characteristics of a blade prepared from the new airfoil

Profile type	INDTH8
Optimal angle of attack	7
Lift coefficient	1.29
Drag coefficient	0.0143697
Blade length	1 m
Hub radius	0.2 m
Number of blades	3
Design wind speed	7 m/s
Optimal design tip speed ratio (λ)	7
Axis of rotation	Horizontal

and the turbine rotor is given by:

$$a = \frac{1}{1 + \frac{4\sin^2\varphi}{\sigma' \times C_L \times COS\varphi}} = \frac{1}{1 + \frac{4\sin^2 27.01}{0.34 \times 1.29 \times COS27.01}} = 0.32 \tag{17}$$

The tangential induction factor (a which is the partial decrease in tangential component of wind velocity between the freestream and the turbine rotor is given by:

$$a' = \frac{1 - 3a}{4a - 1} = \frac{1 - 3 \times 0.32}{4 \times 0.32 - 1} = 0.14 \tag{18}$$

Pitch angle (θ_p) is defined as the difference between relative angle (φ) and angle of attack (α). For the present case, pitch angle $\theta_p = \varphi - \alpha = 27.01^0 - 7^0 = 20.01°$

Manwell et al. [5] reported local tip speed ratio as:

$$N_{rotor} = \frac{30}{\pi}\lambda\frac{V}{R} \tag{19}$$

where, N_{rotor}: Rotational speed of turbine; λ: Tip Speed Ratio; V: Wind speed; R: Radius of rotor. At average wind speed $v = 7$ m/s, $R = 1.2$ m and $\lambda = 7$, the rotational speed calculated from Eq. (19) is approximately 391 rpm. Hence, the selected range for simulation of micro-capacity wind turbine is taken within the range of 200–500 rpm. Many researchers also have reported the experimental as well as simulation results for micro-capacity wind turbines up to rotor speed of 500 rpm [4, 16].

Table 4 shows different parameters of wind turbine blade design for INDTH8 airfoil. The local radius for the element is varied from 200 to 1200 mm with a step size of 100 mm. based on these input parameters, various blade design parameters such as chord length, blade thickness, relative angle, solidity, induction factors, and pitch angle are calculated. The entire rotor blade span is divided into ten segments. The chord length is decreasing towards the trailing edge.

At a tip speed ratio of 7, from the analysis the INDTH8 airfoil at a low Reynolds number shows better results compared to other airfoils. Wind turbine rotor blade design BEM Simulation is carried out. From simulation results, various plots are obtained such as the power coefficient (C_P) versus Tip Speed Ratio (TSR) and thrust coefficient (C_T) versus tip speed ratio (TSR). Define the turbine simulation at the Tip Speed Ratio span from 1 to 17 with a step size increment of 0.5.

Figure 6 communicates the alteration of the power coefficient versus TSR for blades made by different airfoils. Turbine simulation is accomplished at $Re = 500{,}000$. At lower TSR, the alteration in the power coefficient is less. In the range of 3–8 TSR, the lift coefficient increases quickly and after that alteration in the lift coefficient is less. The maximum power coefficient that is obtained for a blade made

Table 4 Design parameters of rotor blade of the INDTH 8 airfoil

S. no	Local radius r (mm)	Local TSR λ_r	Chord length c (mm)	Thickness in (mm)	Relative angle φ (°)	Solidity σ'	Axial induction factor a	Tangential induction factors a'	Pitch angle $\theta_{p\,(°)}$
1	200	1.17	142.3	12.62	27.07	0.339	0.320	0.140	20.1
2	300	1.75	115.5	10.25	19.83	0.184	0.326	0.067	12.8
3	400	2.33	94.06	8.34	15.47	0.112	0.329	0.039	8.47
4	500	2.92	78.40	6.95	12.62	0.075	0.331	0.025	5.62
5	600	3.5	66.87	5.93	10.63	0.053	0.331	0.018	3.63
6	700	4.08	58.15	5.16	9.174	0.031	0.332	0.013	2.17
7	800	4.67	51.36	4.56	8.063	0.031	0.332	0.010	1.06
8	900	5.25	45.95	4.08	7.181	0.024	0.332	0.008	0.19
9	1000	5.83	41.55	3.69	6.485	0.011	0.333	0.006	− 0.5
10	1100	6.42	37.91	3.36	5.905	0.016	0.333	0.005	− 1.1
11	1200	7	34.84	3.09	5.420	0.014	0.333	0.005	− 1.6

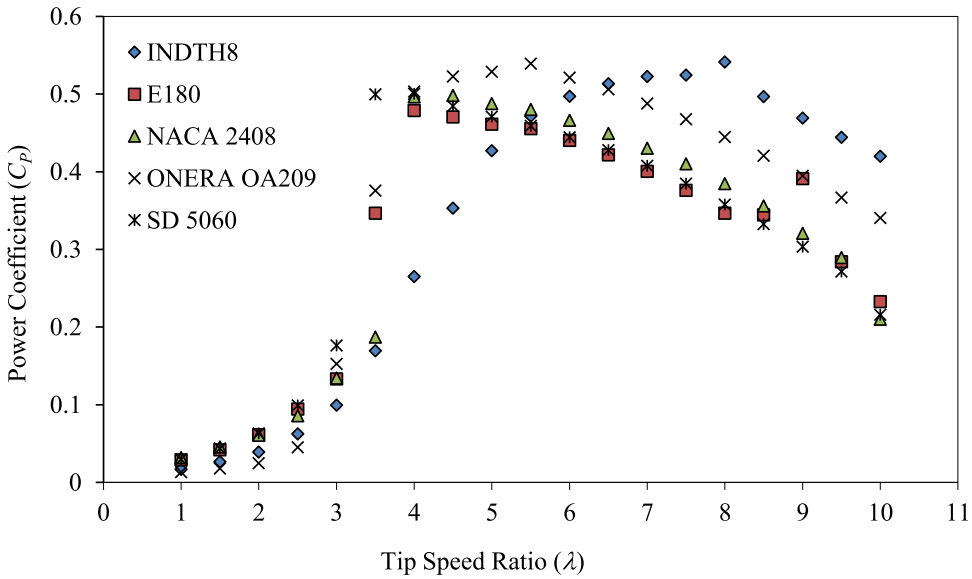

Fig. 6 Plot of power coefficient versus tip speed ratio for the different airfoils

of INDTH8 airfoil is 0.522 at a TSR of 7. Similarly, airfoil E180, NACA 2408, ONERA OA209, and SD 5060 have power coefficients 0.478894 at TSR 4, 0.498 at TSR 4.5, 0.539116 at TSR 5.5 and 0.500444 at TSR 4 respectively. For INDTH8 airfoil notable power coefficient is high which results in maximum power output. Hence INDTH8 airfoil will be a befitting option for micro-capacity wind turbine blades. According to Osei et al. [26], primary wind turbine rotor simulation showed for the airfoil series under study viz. EYO7-8, 8-8, and 9-8 rotors noted maximum power coefficients below 0.371. In order to do this study, the results obtained for the INDTTH8 airfoil rotor blade show better outcomes in comparison with this airfoil series. At very high TSR ($\lambda = 10 - 12$), the rotor rotates so quick that it views the wind as a completely blocked disc. The wind glides around this disc (a solid disc), so there is no wind transport through the rotor, and hence no probability to withdraw power from a motile wind.

The adaptation of the thrust coefficient with tip speed ratio formulates following outcomes. It is found that the thrust coefficient obtained for INDTH8 airfoil is in better agreement with airfoils considered under study. The value of the coefficient of thrust is 0.8 at TSR of 7. From the simulation consequence it is found that the power coefficient (CP) and Thrust Coefficient (C_T) for INDTH8 airfoil is 0.52 and 0.8 at a TSR of 7.

The variation in power yield with respect to variation in speed for INDTH8 shows following outputs. In this simulation, at a wind speed of 7 m/s, the power output is of the order of 176.768 W. As wind speed increases, power output will increase as the power output is proportionate to 3rd power of the velocity. Similarly, power output can be obtained for

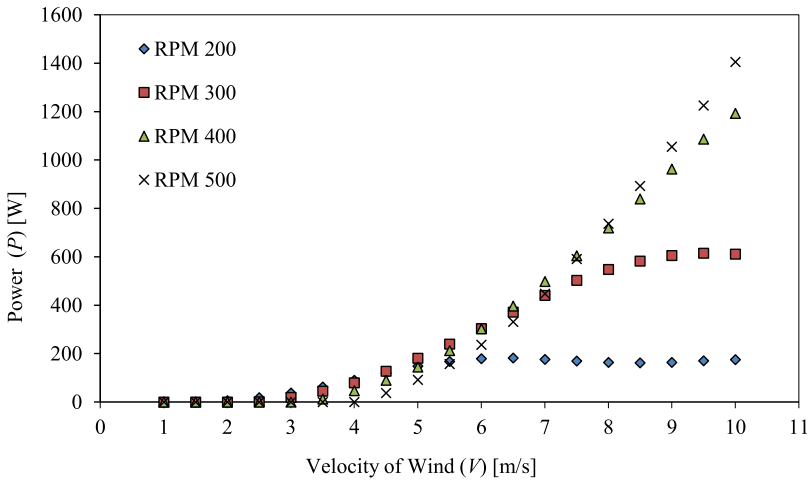

(a) Plot of power versus wind speed for the INDTH8 airfoil

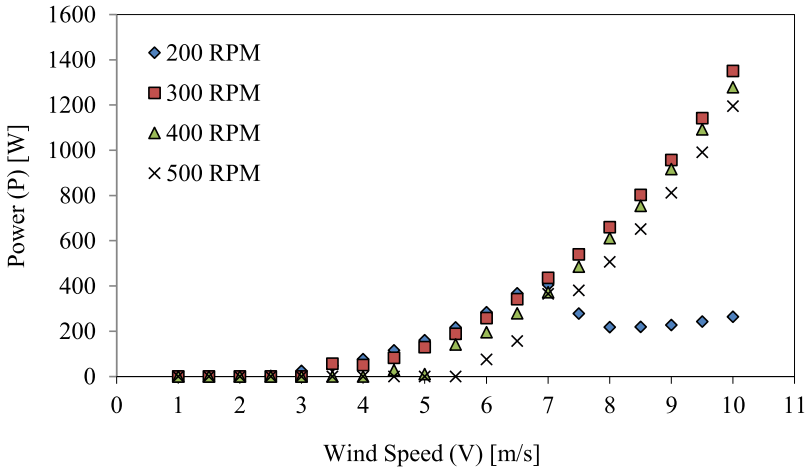

(b) Power versus wind speed for the E180 airfoil

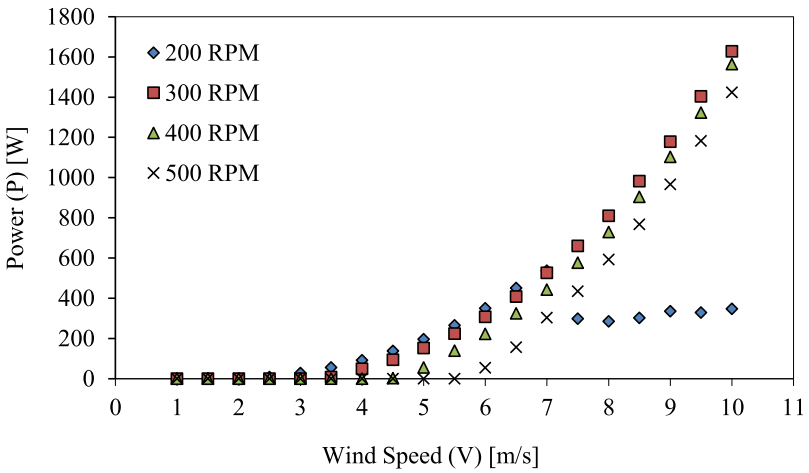

(c) Power versus wind speed for the NACA2408 airfoil

Fig. 7 **a** Plot of power versus wind speed for the INDTH8 airfoil, **b** Power versus wind speed for the E180 airfoil, **c** Power versus wind speed for the NACA2408 airfoil, **d** Power versus wind speed for the ONERA OA209 airfoil, **e** Power versus wind speed for the SD5060 airfoil

Fig. 7 continued

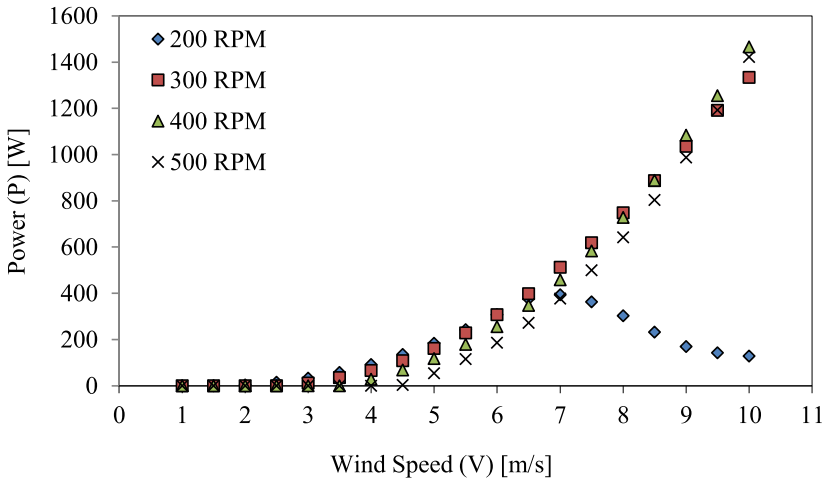

(d) Power versus wind speed for the ONERA OA209 airfoil

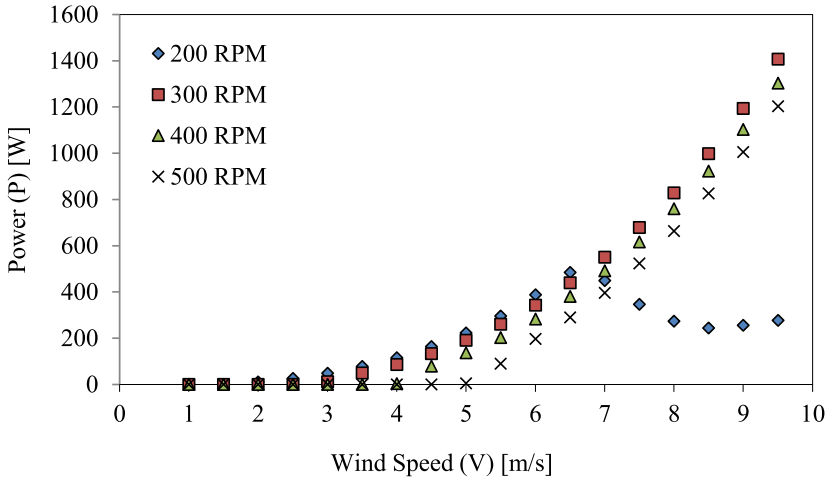

(e) Power versus wind speed for the SD5060 airfoil

different rotational speeds of 200, 300, 400, and 500 rpm for all the airfoils under consideration as shown in Fig. 7a–e.

From Fig. 7a, the INDTH8 airfoil shows a plot of power versus wind speed for different ranges of rotational speed (200–500) rpm. The entire simulation is carried out for variation in the wind speed of 1–10 m/s. Cut-in speed is the speed below which the turbine can't produce electricity. The cut-in speed for the INDH8 airfoil turbine is estimated as 2 m/s for 200 rpm. Similarly, it is noted that for the range of (300, 400 and 500) rpm the cut-in speed is (2.5, 3.5, and 4.5) m/s respectively. As the wind speed increases, the output power starts increasing till it reaches the rated value of the generator. Rated wind speed is the speed concerning maximum power generation is achieved. The rated speed noticed for the INDTH8 airfoil turbine is 7 m/s at 200 rpm. With the augment of rotational speed from 300, 400, and 500 rpm, the values of rated wind speed obtained are 9.5, 10, and 10 m/s respectively. When the wind speed increases above the cut-off speed, the turbine is closed down for safety purposes. The rated power obtained is 176.76, 615.27, 1192.49, and 1405.33 W for 200, 300, 400, and 500 rpm respectively.

Power versus wind speed simulation is carried out for the E180 airfoil turbine at TSR of 1–10, wind speed range of 1–10 m/s, and at different rotational speeds i.e. 200–500 rpm. Cut-in and rated speeds noted at 200 rpm are 2.5 and 7 m/s respectively. It is noted that for the range of 300, 400, and 500 rpm, the cut-in speed is 3.5, 4.5, and 6 m/s respectively. Similarly, it is noted that for the range of 300 to 500 rpm, the rated speed is 10 m/s. From Fig. 7b, it is noted that the rated power is: 404.39, 1349.82, 1278.55, and 1194.23 W for the rotational speeds of 200, 300, 400, and 500 rpm respectively. If the cut-in speed exceeds 5 m/s in such cases design airfoil

is not befitting for low wind speed site conditions. According to Bukala et al. [32], developing a wind turbine for low- speed surroundings of 4-5 m/s is economically unjustified.

Power versus wind speed simulation is carried out for the NACA2408 airfoil turbine at TSR of 1– 10, wind speed range of 1–10 m/s, and at different rotational speeds in the range of 200–500 rpm. For rotational speed of 200 rpm, cut-in and rated speeds for NACA2408 airfoil turbine simulation are noted as 2.5 and 7 m/s respectively. Cut-in speeds obtained for the 300 rpm, 400 rpm, and 500 rpm are 3.5, 4.5 and 6 m/s respectively. Outcome signifies that for constant radii of rotation increase in rotational speed, cut in speed will increase. Power versus wind speed at different rpm shows alteration of power with respect to cut-in speed, rated speed, and cut-out speed which is very impactful forecasting for windmill power plants. The behavior of the plot looks exponentially proportional. Wind speed is one of the influencing factors in wind power capacity estimation. At high wind speed conditions turbine works on the principle of constant speed, in such circumstances pitch angle comes into the picture and controls the speed of the rotor as constant. Output power for the turbine working in this mode is 3rd power of rotor speed till it approaches as rated speed.

From Fig. 7c, it is noted that the rated powers are: 536.841 W, 1627.44 W, 1564.09 W, and 1423.49 W at rotational speeds of 200 rpm, 300 rpm, 400 rpm, and 500 rpm respectively.

Power versus wind speed simulation is conducted for the ONERA OA209 airfoil turbine at TSR of 1–10, wind speed range of 1–10 m/s, and different rotational speeds ranging between 200 and 500 rpm. For rotational speed of 200 rpm, cut-in and rated speed for ONERA OA209 airfoil turbine simulation are noted as 2 and 7 m/s respectively. There is very much similarity in the obtained results of NACA2408 and ONERA OA209 airfoil. For rotational speed in the range of (300–500) rpm power curve increases with an increase in wind speed. After attending rated power at rated speed turbine moves towards cut-off speed, this is because turbines are designed for certain mechanical loads. Here the objective is to reduce these loads on the blades as well on the tower. Otherwise lifting will destroy the turbine. So for this reason operating speed is reduced up to a point beyond the cut-out speed. Every turbine must have a rotating speed limit. From Fig. 7d, it is noted that the rated powers obtained are: 392.72 W, 1333.15 W, 1466.11 W, and 1422.58 W for 200, 300, 400 and 500 rpm respectively.

Power versus wind speed simulation is conducted for the SD5060 airfoil turbine at a TSR range of 1–10, wind speed range of 1–10 m/s, and different rotational speeds i.e. 200–500 rpm. For the rotational speed of 200 rpm, cut-in and rated speed for the SD5060 airfoil turbine simulation are noted as 2.5 m/s and 7 m/s respectively. To understand the wind speed region-wise graphical phenomena, region 1st is wind speed (0 to cut-in), region 2nd is (cut-in to rated), region 3rd is (rated to cut-off), and region 4th is (above cut-off). The rated speed noted for (300–500) rpm is 10 m/s. From Fig. 7e it is noted that the rated powers obtained for the SD5060 airfoil are: 484.017 W, 1406.27 W, 1303.28 W, and 1202.68 W at (200–500) rpm, rpm respectively.

4 Conclusions

From the current study, the following findings can be described:

The INDTH8 airfoil reported a ratio of lift to drag coefficient (CL/CD) equal to 89.86 at Re $= 5\times10^5$ which is higher than any other airfoil for the same Reynolds number. The maximum power coefficient for the INDTH8 airfoil is obtained as 0.52 at a tip-speed ratio of 7. It is observed from the analysis that the maximum lift/drag coefficient is 89.86 at an angle of attack of 7°.

It is observed that at an average wind speed of 7 m/s, at various rpm viz. 200, 300, 400, and 500, the maximum obtainable powers are in the order of 176.768 W, 441.265 W, 498.356 W, and 447.194 W respectively. At an average wind speed of 7 m/s and 5 TSR for 500 rpm, INDTH8 shows power in the range of 447.18 W, E180 shows 364.62 W, NACA 2408 shows 302.6 W, ONERA OA 209 produces 376.56 W.

INDTH8 airfoil shows better results among all airfoils. The lift coefficient is 0.6 for AOA 0° and it is 1.6849 for AOA 13.5°.Sall angle for INDTH8 airfoil is obtained as13.5° similarly for airfoils E180, NACA2408, ONERAOA209, and SD5060 it is noted as 10.5°, 10°, 14° and 11°.

Performance run shows that the lift coefficient of all airfoils under study was relatively rendered insensible to changes in 300000 $\leq$ Re $\leq$ 500000. Maximum lift coefficient noted at Re $=$ 500000 for airfoil INDTH8 as 1.6849 whereas for airfoils—E180, NACA 2408, ONERA OA209, and SD5060 It is noted as 1.135, 1.013, 1.383, and 1.323 respectively.

The streamlined performance of the INDTH8 airfoil is worthy for use in micro-capacity wind turbine blades mainly within the Re range of 300,000 and 500,000 owing to the less contrast in lift loading circumstances within same range.

Author contributions Mr. MLS Conducting of the computational work, Dr. PDD the data acquisition and analysis, Dr. KBS: Conception, interpretation of data, drafted the work and revised it, Dr. BSK design of the work, Dr. KSB Conducting of the computational work.

Funding The authors declare that no funds, grants, or other support were received during the preparation of this manuscript.

Declarations

Conflict of interest The authors have no relevant financial or non-financial interests to disclose.

References

1. Renewable Energy Capacity Statistics 2022.: International Renewable Energy Agency. file:///C:/Users/Aniruddh/Downloads/IRENA_RE_Capacity_Statistics_2022.pdf Accessed on: 3rd July, 2022
2. Wind Energy Overview.: Ministry of new and renewable energy. https://mnre.gov.in/wind/current-status/. Accessed on: 23rd May, 2023
3. Rahman, M.M., Baky, M.A.H., Islam, A.K.M.S.: Electricity from wind for off-grid applications in Bangladesh: a techno-economic assessment. Int. J. Renew. Energy Dev. **6**(1), 55–64 (2017). https://doi.org/10.14710/ijred.6.1.55-64
4. Tummala, A., Velamati, R.K., Sinha, D.K., Indraja, V., Krishna, V.H.: A review on small scale wind turbines. Renew. Sustain. Energy Rev. **56**, 1351–1371 (2016). https://doi.org/10.1016/j.rser.2015.12.027
5. Manwell, J.F., McGowan, J.G., Rogers, A.L.: Wind Energy Explained: Theory, Design and Application. Wiley, New York (2010)
6. QBlade: next generation wind turbine design and simulation. https://qblade.org/ . . Cited on: 23rd May, 2023
7. Marten, D., Wendler, J., Pechlivanoglou, G., Nayeri, C.N.: CoP. QBLADE: an open source tool for design and simulation of horizontal and vertical axis wind turbines. Int. J. Emerg. Technol. Adv. Eng. **3**(3), 264–269 (2013)
8. XFOIL: Subsonic airfoil development system. https://web.mit.edu/drela/Public/web/xfoil/. Cited on: 23rd May, 2023
9. Koç, E., Günel, O., Yavuz, T.: Comparison of Qblade and CFD results for small- scaled horizontal axis wind turbine analysis. In: IEEE International Conference on Renewable Energy Research and Applications (ICRERA), pp. 204–209. https://doi.org/10.1109/ICRERA.2016.7884538(2016)
10. Dhurpate, P.: Numerical analysis of different airfoils using QBlade software. Imperial J. Interdiscip. Res. 2(6). http://www.onlinejournal.in/IJIRV2I6/264.pdf (2016)
11. Giguere, P., Selig, M.S.: New airfoils for small horizontal axis wind turbines. J. Solar Energy Eng. Trans. ASME **120**, 108–114 (1998). https://doi.org/10.1115/1.28880
12. Lee, M.H., Shiah, Y.C., Bai, C.J.: Experiments and numerical simulations of the rotor-blade performance for a small-scale horizontal axis wind turbine. J. Wind Eng. Ind. Aerodyn. **149**, 17–29 (2016). https://doi.org/10.1016/j.jweia.2015.12.002
13. Akour, S.N., Al-Heymari, M., Ahmed, T., Khalil, K.A.: Experimental and theoretical investigation of micro wind turbine for low wind speed regions. Renew. Energy **116**, 215–223 (2018). https://doi.org/10.1016/j.renene.2017.09.076
14. Almohammadi, K.M.: Assessment of several modeling strategies on the prediction of lift-drag coefficients of a NACA0012 airfoil at a moderate Reynold number. Alex. Eng. J. **61**(3), 2242–2249 (2022). https://doi.org/10.1016/j.aej.2021.07.008
15. Blackwood, M.: Maximum efficiency of a wind turbine. Undergrad. J. Math. Model. One Two **6**(2), 2 (2016)
16. Singh, R.K., Ahmed, M.R., Zullah, M.A., Lee, Y.H.: Design of a low Reynolds number airfoil for small horizontal axis wind turbines. Renew. Energy **42**, 66–76 (2012). https://doi.org/10.1016/j.renene.2011.09.014
17. Karasu, I., Açıkel, H.H., Koca, K., Genç, M.S.: Effects of thickness and camber ratio on flow characteristics over airfoils. J. Therm. Eng. **6**, 242–252 (2020). https://doi.org/10.18186/thermal.710967
18. Karthikeyan, N., Murugavel, K.K., Kumar, S.A., Rajakumar, S.: Review of aerodynamic developments on small horizontal axis wind turbine blade. Renew. Sustain. Energy Rev. **42**, 801–822 (2015). https://doi.org/10.1016/j.rser.2014.10.086
19. Saryazdi, S.M.E., Boroushaki, M.: 2D numerical simulation and sensitive analysis of h-darrieus wind turbine. Int. J. Renew. Energy Dev. **7**(1), 23 (2018). https://doi.org/10.14710/ijred.7.1.23-24
20. NACA 2408 airfoil. Airfoil tool. http://airfoiltools.com/airfoil/details?airfoil=naca2408-il. Accessed on: 4th Aug 2021
21. ONERA/Aerospatiale OA209 rotorcraft airfoil. Airfoil tool. http://airfoiltools.com/airfoil/details?airfoil=oa209-il. Accessed on: 4th Aug 2021
22. Eppler E180 low Reynolds number airfoil. *Airfoil tool.* http://airfoiltools.com/airfoil/details?airfoil=e180-il Accessed on: 4th Aug. 2021
23. Selig/Donovan SD5060 low Reynolds number airfoil. Airfoil tool. http://airfoiltools.com/airfoil/details?airfoil=sd5060-il. Accessed on: 4th Aug. 2021
24. Cousteix, T.C.J., Cebeci, J.: Modeling and Computation of Boundary-Layer Flows. Springer, Berlin, Heidelberg (2005)
25. Yining, Y.: Analysis of the influence of camber on hydrodynamic characteristics of airfoil based on FLUENT. J. Phys. Conf. Ser. **1519**(1), 012020 (2020). https://doi.org/10.1088/1742-6596/1519/1/012020
26. Osei, E.Y., Opoku, R., Sunnu, A.K., Adaramola, M.S., Kyeremeh, E.A.: Aerodynamic performance characteristics of EYO-Series low Reynolds number airfoils for small wind turbine applications. Alex. Eng. J. **61**(12), 12301–12310 (2022). https://doi.org/10.1016/j.aej.2022.05.049
27. Kale, S.A., Birajdar, M.R., Sapali, S.N.: Numerical analysis of new airfoils for small wind turbine blade. J. Altern. Energy Sour. Technol. **6**(1), 1–6 (2016)
28. Lee, H., Lee, D.J.: Low Reynolds number effects on aerodynamic loads of a small scale wind turbine. Renew. Energy **154**, 1283–1293 (2020). https://doi.org/10.1016/j.renene.2020.03.097
29. Surve, M., Deshmukh, P.D., Purohit, H.: Design and Analysis of New Airfoil and Blade for Micro- Capacity Horizontal Axis Wind Turbine Using QBlade Tool. In: 5th International Conference on Advances in Science and Technology (ICAST), Mumbai, India, pp. 531–536, https://doi.org/10.1109/ICAST55766.2022.10039645 (2022)
30. Burton, T., Jenkins, N., Sharpe, D., Bossanyi, E.: Wind Energy Handbook. Wiley, New York (2011)
31. Piggott, H.: Wind power workshop. Building your own wind turbine (1997)
32. Bukala, J.K., Kroszczynski, K., Krzeszowiec, M., Malachowski, J.: Investigation of parameters influencing the efficiency of small wind turbines. J. Wind Eng. Ind. Aerodyn. **146**, 29–38 (2015). https://doi.org/10.1016/j.jweia.2015.06.017